JOURNAL OF THERMOPHYSICS AND HEAT TRANSFER
Vol. 9, No. 2, April–June 1995

Theoretical Investigation of Particles Having Directionally Dependent Absorption Cross Section

Daniel W. Mackowski* and Peter D. Jones*
Auburn University, Auburn, Alabama 36849

Examined here are a class of particles that possess highly anisotropic absorption cross sections. The particles are in the form of an eccentrically stratified sphere in which a relatively small, highly absorbing sphere is located against the interior surface of a larger, nonabsorbing sphere. For this configuration the nonabsorbing sphere can act essentially as a lens and focus radiation onto the absorbing sphere. Using an exact solution to Maxwell's wave equations, the directionally-dependent absorption cross sections of the particle are predicted for refractive indices of common absorbing and nonabsorbing materials and radiative size parameters ranging from 5 to 50. Under certain conditions, the absorption cross section of the particle can be extremely sensitive to the direction of the incident radiation. Placing the absorber opposite the point of incidence can result in an absorption cross section that is two orders of magnitude greater than its isolated, single-particle value, yet for incident angles as little as 20 deg removed from the focused condition, the absorption becomes comparable to or smaller than the isolated value. Factors that optimize the absorption anisotropy and the implications with regard to radiative transfer are discussed.

Nomenclature

A_{mnml}, B_{mnml}	=	addition coefficients
a_{mn}, b_{mn}	=	scattering expansion coefficients
$\bar{a}_n$, $\bar{b}_n$	=	scattered field Lorenz/Mie coefficients
c_{mn}, d_{mn}	=	internal field expansion coefficients
$\bar{c}_n$, $\bar{d}_n$	=	internal field Lorenz/Mie coefficients
E	=	electric field
E_{mn}	=	normalization factor
$\bar{f}_n$, $\bar{g}_n$	=	layered sphere Lorenz/Mie coefficients
k	=	wave number, $2\pi/\lambda$
$\boldsymbol{M}_{mn}$, $\boldsymbol{N}_{mn}$	=	vector harmonics
m_i	=	refractive index of sphere i, $n + ik$
p_{mn}, q_{mn}	=	incident field expansion coefficients
Q	=	efficiency factor
$\bar{u}_n$, $\bar{v}_n$	=	layered sphere Lorenz/Mie coefficients
X_{1-2}	=	nondimensional separation distance, kR_{1-2}
x	=	size parameter ka
β	=	incident angle
γ	=	polarization angle
θ	=	scattering polar angle
π_{mn}, τ_{mn}	=	scattering functions
Φ	=	scattering phase function
ϕ	=	scattering azimuthal angle

Subscripts

abs	=	absorption
ext	=	extinction
i	=	internal
s	=	scattered
sca	=	scattering
0	=	external or incident
1	=	sphere 1
2	=	sphere 2

Introduction

IN two recent papers, Fuller has presented examinations of the electromagnetic scattering properties of two-sphere systems, in which a relatively small absorbing sphere resides either on the exterior surface[1] or within[2] a larger, nonabsorbing sphere. A fascinating result of his work was the degree to which the absorption cross section of the system was dependent on the direction of the incident radiation. This behavior results from the focusing ability of the nonabsorbing sphere, in that radiation entering the sphere becomes concentrated into a region directly opposite the point of incidence. When the smaller, absorbing sphere is situated in this focal region the absorption cross section of the entire system can greatly exceed that predicted for the absorbing sphere alone. Furthermore, rotating the system a small amount with respect to the incident beam results in the removal of the absorber from the focal region and a concurrent sharp decrease in absorption.

The primary motivation behind Fuller's work was the prediction of radiative properties of atmospheric aerosols consisting of carbon particles attached to water or sulfate droplets. Since the aerosols will be randomly oriented, the orientation-averaged quantities are of practical interest in this application. However, the directionally-dependent absorption behavior was especially interesting, and led us to consider the propagation of radiation through a hypothetical medium having an anisotropic bulk absorption coefficient. In principle, the medium could be devised from a matrix of anisotropic absorbing particles, all with a set orientation in the medium. Such a medium would have intriguing behavior. Not only would it preferentially absorb radiation propagating in a particular direction, it would also preferentially emit radiation in the opposite direction. This behavior could be of significant benefit in many engineering applications, e.g., radiant burners, high-temperature insulation, and solar collectors.

The objective of this article and its companion[3] is to examine the nature of radiative transfer through a hypothetical anisotropically absorbing medium. This article addresses the microscopic elements of the problem by proposing a "model" of an anisotropically absorbing particle and predicting the absorption and scattering properties of the particle as a function of incident direction. In the companion article we couple the information obtained herein into a macroscopic analysis of radiative heat transfer through the medium. We should emphasize that our motivation at this point is merely academic—the technological problems associated with fabricating anisotropically absorbing particles and (especially) orienting them in a medium are likely to be insurmountable in

Received June 17, 1994; revision received Sept. 9, 1994; accepted for publication Sept. 12, 1994.

*Assistant Professor, Mechanical Engineering Department. Member AIAA.

the near future. We hope, though, that the results presented in these two articles will spur interest in this topic.

Model and Analysis

Particle Model

As discussed by Fuller,[1,2] a two-sphere system can produce a directionally-dependent absorption coefficient. In this article we focus on the situation in which the absorbing sphere is located inside the nonabsorbing sphere (Fig. 1). Essentially, the system can be thought of as an eccentrically layered sphere. We have made calculations for both internal and external placements of the absorbing sphere, and concluded that the internal placement offered slightly better absorption anisotropy than the external case. In addition, this configuration would likely be easier to fabricate—perhaps through condensation of the vapor phase nonabsorbing material onto the absorber, and allowing density differences to eccentrically align the absorber.

Providing that the diameters of both spheres are significantly greater than the wavelength of the incident radiation, the absorption and scattering properties of the system can be determined through geometrical optics (or, equivalently, ray-tracing) techniques.[4,5] Such an approach would, however, place constraints on the allowable size of the smaller absorbing sphere, and to avoid these limitations we analyze the system using the exact solution of Maxwell's wave equations. A solution method for the wave equations as applied to neighboring spheres was actually developed over 20 yr ago,[6] yet calculation of the solution has only recently become approachable due to advances in both the formulation and computational resources. The reader is referred to works by Borghese et al.,[7] Fuller,[8] and Mackowski[9] for overviews of the formulation for external spheres. The analysis of eccentrically stratified spheres has been presented by Fikioris and Uzunoglu,[10] Borghese et al.,[11] and Fuller.[2] In general, the solution method for both cases involves a superposition formulation in which the field produced by the system is constructed, when appropriate, as a superposition of fields expanded about each of the sphere origins in the system.

To set up the problem, we first define the key properties and parameters of the system. Each of the spheres is characterized by a nondimensional size parameter $x_1 = ka_1$ and $x_2 = ka_2$, in which $k = 2\pi/\lambda$ is the wave number of the incident radiation, and a is the radius, and a complex index of refraction $m_1 = n_1 + ik_1$ and $m_2 = n_2 + ik_2$. Sphere 1 is taken to be centered on the origin of the system, and the z axis of the system is taken to be fixed to the line connecting the two spheres. Sphere 2 lies on the positive z axis a distance R from the origin, and $X_{1-2} = kR$ denotes the nondimensional separation distance of the sphere centers. The incident radiation, which is taken to be a plane wave, propagates along the $x - z$ plane of the system, and intersects the z axis at an angle β. The electric field vector of the incident radiation is linearly polarized at an angle γ with respect to the $x - z$ plane.

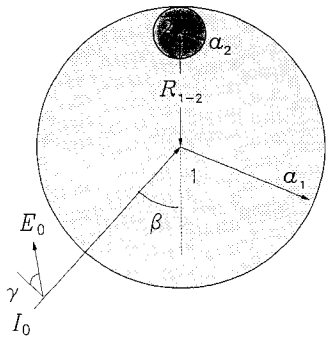

Fig. 1 Particle model.

Solution of Wave Equations

The solution presented here for electromagnetic scattering by an eccentrically stratified sphere follows that developed by Borghese et al.[11] and Fuller.[2] Only the salient aspects of the solution are presented; details of the analysis can be found in Refs. (11) and (2). Using the notation of Bohren and Huffman,[4] the scattered electric field from the system is represented by an expansion of vector harmonics about the origin of sphere 1:

$$\boldsymbol{E}_s = \sum_{m,n} [a_{mn,1}\boldsymbol{N}^{(3)}_{mn}(r_1) + b_{mn,1}\boldsymbol{M}^{(3)}_{mn}(r_1)] \tag{1}$$

In Eq. (1), a_{mn} and b_{mn} are as-of-yet undetermined expansion (or scattering) coefficients, the summation is taken over $m = -n, -n+1, \ldots n$; $n = 1, 2, \ldots \infty$, $\boldsymbol{M}$ and $\boldsymbol{N}$ represent vector harmonics, and r_1 denotes the spherical coordinates r_1, θ_1, and ϕ_1. The superscript (3) on $\boldsymbol{M}$ and $\boldsymbol{N}$ denotes that the harmonics are based on the spherical Hankel function $h_n(kr_1)$, which yields the correct far-field behavior. Within sphere 2, the internal electric field $E_{i,2}$ is described by a similar expansion, except now written about the origin of 2

$$\boldsymbol{E}_{i,2} = \sum_{m,n} [d_{mn,2}\boldsymbol{N}^{(1)}_{mn}(m_2r_2) + c_{mn,2}\boldsymbol{M}^{(1)}_{mn}(m_2r_2)] \tag{2}$$

in which the superscript (1) on $\boldsymbol{M}$ and $\boldsymbol{N}$ denotes that the harmonics are now based upon the spherical Bessel functions of $j_n(m_2kr_2)$, which remains finite at the origin of sphere 2. In the region external to sphere 2 and internal to sphere 1, the field is taken as a superposition of a scattered field about origin 2 and internal field about origin 1. Denoting this region 1′, the superposition can be stated

$$\boldsymbol{E}_{1'} = \boldsymbol{E}_{i,1} + \boldsymbol{E}_{s,2} \tag{3}$$

The field $E_{i,1}$ is given by Eq. (2) with subscripts denoting sphere 2 changed to 1, whereas the expansion for $E_{s,2}$ must now take into account that the medium has a refractive index of m_1. Consequently,

$$\boldsymbol{E}_{s,2} = \sum_{m,n} [a_{mn,2}\boldsymbol{N}^{(3)}_{mn}(m_1r_2) + b_{mn,2}\boldsymbol{M}^{(3)}_{mn}(m_1r_2)] \tag{4}$$

Finally, the incident electric field E_0 is expanded about the origin of 1 via

$$\boldsymbol{E}_0 = -\sum_{m,n} [p_{mn}\boldsymbol{N}^{(1)}_{mn}(r_1) + q_{mn}\boldsymbol{M}^{(1)}_{mn}(r_1)] \tag{5}$$

where the coefficients p_{mn} and q_{mn} depend on β and γ, and are given by

$$\begin{aligned} p_{mn} &= -i^{n+1}(1/2E_{mn})[\tau_{mn}(\beta)\cos\gamma - i\pi_{mn}(\beta)\sin\gamma] \\ q_{mn} &= -i^{n}(1/2E_{mn})[\tau_{mn}(\beta)\sin\gamma + i\pi_{mn}(\beta)\cos\gamma] \end{aligned} \tag{6}$$

in which

$$E_{mn} = \frac{n(n+1)}{2n+1}\frac{(n+m)!}{(n-m)!} \tag{7}$$

The scattering functions π_{mn} and τ_{mn} are related to the associated Legendre function P^m_n by

$$\begin{aligned} \tau_{mn}(\beta) &= \frac{\mathrm{d}}{\mathrm{d}\beta}P^m_n(\cos\beta) \\ \pi_{mn}(\beta) &= \frac{m}{\sin\beta}P^m_n(\cos\beta) \end{aligned} \tag{8}$$

The corresponding magnetic field for the above expansions is given by $\boldsymbol{H} = (\nabla \times \boldsymbol{E})/i\omega\mu$, where ω and μ are the circular

frequency and magnetic permeability, respectively. Using the relation $\boldsymbol{M} = \nabla \times \boldsymbol{N}$, the magnetic field can be written in vector harmonic expansions similar to those for the electric fields.

The boundary conditions have the tangential components of the electric and magnetic fields continuous at the surface of each sphere. Because of the superposition in Eq. (3), the contributions of the field at each surface will contain harmonics centered about both of the sphere origins. To exploit the orthogonality properties of the vector harmonics in satisfying the boundary condition at each surface, it is thus necessary to transform the harmonics centered about one origin into harmonics centered about the other origin. This is accomplished using the addition theorem for vector spherical harmonics, which states that a harmonic about one origin can be expressed as an expansion of harmonics about another origin. By incorporating the addition theorem into the boundary conditions at each surface, and after truncating the field expansions about spheres 1 and 2 after N_1 and N_2 orders, a linear system of equations can be developed for the sphere 2 scattering coefficients and the sphere 1 internal coefficients. These equations are

$$d_{mn,1} = \bar{d}_{n,1} p_{mn,1} - \bar{f}_{n,1} \sum_{l=\max(1,|m|)}^{N_2} (-1)^{n+l} (A_{mlnn} a_{ml,2} - B_{mlnn} b_{ml,2}) \tag{9}$$

$$c_{mn,1} = \bar{c}_{n,1} q_{mn,1} - \bar{g}_{n,1} \sum_{l=\max(1,|m|)}^{N_2} (-1)^{n+1} (A_{mlnn} b_{ml,2} - B_{mlnn} a_{ml,2}) \tag{10}$$

$$a_{mn,2} = \bar{a}_{n,2} \sum_{l=\max(1,|m|)}^{N_1} (A_{mlnn} d_{ml,1} + B_{mlnn} c_{ml,1}) \tag{11}$$

$$b_{mn,2} = \bar{b}_{n,2} \sum_{l=\max(1,|m|)}^{N_1} (A_{mlnn} c_{ml,1} + B_{mlnn} d_{ml,1}) \tag{12}$$

The tensors A_{mlnn} and B_{mlnn} in the above equations are referred to as the addition coefficients and depend entirely on $m_1 X_{1-2}$. Methods for calculating the addition coefficients using recurrence relations are given in the Appendix. Note that an independent system of equations is obtained for each degree m, with $m = 0, \pm 1, \pm 2, \ldots, \pm N_2$. This is a unique feature of the axial symmetry of the system. The scattered and internal field coefficients for sphere 1 are related by

$$a_{mn,1} = \left(\bar{u}_{n,1} p_{mn} + \frac{\bar{d}_{n,1} d_{mn,1}}{m_1} \right) \frac{1}{\bar{f}_{n,1}} \tag{13}$$

$$b_{mn,1} = \left(\bar{v}_{n,1} q_{mn} + \frac{\bar{c}_{n,1} c_{mn,1}}{m_1} \right) \frac{1}{\bar{g}_{n,1}} \tag{14}$$

in which the overlined symbols in the above equations are defined by

$$\bar{a}_{n,2} = \frac{m_2 \psi_n'(m_1 x_2) \psi_n(m_2 x_2) - m_1 \psi_n(m_1 x_2) \psi_n'(m_2 x_2)}{m_2 \xi_n'(m_1 x_2) \psi_n(m_2 x_2) - m_1 \xi_n(m_1 x_2) \psi_n'(m_2 x_2)} \tag{15}$$

$$\bar{b}_{n,2} = \frac{m_1 \psi_n'(m_1 x_2) \psi_n(m_2 x_2) - m_2 \psi_n(m_1 x_2) \psi_n'(m_2 x_2)}{m_1 \xi_n'(m_1 x_2) \psi_n(m_2 x_2) - m_2 \xi_n(m_1 x_2) \psi_n'(m_2 x_2)} \tag{16}$$

$$\bar{d}_{n,1} = \frac{i m_1}{m_1 \xi_n'(x_1) \psi_n(m_1 x_1) - \xi_n(x_1) \psi_n'(m_1 x_1)} \tag{17}$$

$$\bar{c}_{n,1} = \frac{i m_1}{\xi_n'(x_1) \psi_n(m_1 x_1) - m_1 \xi_n(x_1) \psi_n'(m_1 x_1)} \tag{18}$$

$$\bar{f}_{n,1} = \frac{m_1 \xi_n'(x_1) \xi_n(m_1 x_1) - \xi_n(x_1) \xi_n'(m_1 x_1)}{m_1 \xi_n'(x_1) \psi_n(m_1 x_1) - \xi_n(x_1) \psi_n'(m_1 x_1)} \tag{19}$$

$$\bar{g}_{n,1} = \frac{\xi_n'(x_1) \xi_n(m_1 x_1) - m_1 \xi_n(x_1) \xi_n'(m_1 x_1)}{\xi_n'(x_1) \psi_n(m_1 x_1) - m_1 \xi_n(x_1) \psi_n'(m_1 x_1)} \tag{20}$$

$$\bar{u}_{n,1} = \frac{m_1 \psi_n'(x_1) \xi_n(m_1 x_1) - \psi_n(x_1) \xi_n'(m_1 x_1)}{m_1 \xi_n'(x_1) \psi_n(m_1 x_1) - \xi_n(x_1) \psi_n'(m_1 x_1)} \tag{21}$$

$$\bar{v}_{n,1} = \frac{\psi_n'(x_1) \xi_n(m_1 x_1) - m_1 \psi_n(x_1) \xi_n'(m_1 x_1)}{\xi_n'(x_1) \psi_n(m_1 x_1) - m_1 \xi_n(x_1) \psi_n'(m_1 x_1)} \tag{22}$$

In the above, ψ_n and ξ_n are Ricatti-Bessel functions of the first and third kind, and the prime denotes differentiation with respect to the argument. The quantities $\bar{a}_{n,2}$ and $\bar{b}_{n,2}$ are recognized as the Lorenz/Mie scattering and internal field coefficients for a sphere of refractive index m_2 embedded in a medium of refractive index m_1, whereas $\bar{d}_{n,1}$ and $\bar{c}_{n,1}$ are the Lorenz/Mie internal field coefficients for a sphere of refractive index m_1 in a vacuum. The other quantities arise from the analysis of scattering from a concentrically layered sphere.[4,12] Indeed, if $X_{1-2} = 0$ (i.e., the spheres are concentric), the addition coefficients reduce to A_{mlnn} and δ_{ln}, $B_{mlnn} = 0$, and the formulation becomes equivalent to that for a layered sphere.[2] An additional check is when $m_1 = m_2$, for which the formulation will reduce (after some algebra) to the Lorenz/Mie homogeneous sphere solution.

Efficiency Factors and Phase Function

Upon solution of Eqs. (9–14), the radiative efficiency factors for the particle can be obtained from the scattering coefficients via

$$Q_{\text{ext}} = \frac{4}{x_1^2} \sum_{m,n} E_{mn} Re(a_{mn,1} p_{mn}^* + b_{mn,1} q_{mn}^*) \tag{23}$$

$$Q_{\text{sca}} = \frac{4}{x_1^2} \sum_{m,n} E_{mn} (|a_{mn,1}|^2 + |b_{mn,1}|^2) \tag{24}$$

$$Q_{\text{back}} = \frac{4}{x_1^2} \left| \sum_{m,n} (-1)^n E_{mn} (a_{mn,1} p_{mn}^* - b_{mn,1} q_{mn}^*) \right|^2 \tag{25}$$

in which Q_{ext}, Q_{sca}, and Q_{back} denote the extinction, scattering, and backscattering efficiencies, respectively, and the asterisk denotes conjugate. Realize that the efficiencies are defined with respect to sphere 1, so that the cross section C will be given by $C = \pi a_1^2 Q$. The far-field components of the scattered electric field are also given by

$$E_{s,\theta} = \frac{i}{kr} e^{ikr} \sum_{m,n} (-i)^{n+1} [a_{mn,1} \tau_{mn}(\theta) + b_{mn,1} \pi_{mn}(\theta)] e^{im\phi}$$
$$E_{s,\phi} = \frac{-1}{kr} e^{ikr} \sum_{m,n} (-i)^{n+1} [a_{mn,1} \pi_{mn}(\theta) + b_{mn,1} \tau_{mn}(\theta)] e^{im\Phi} \tag{26}$$

and the normalized scattering phase function is

$$\Phi(\theta, \phi) = \frac{r^2 (|E_{s,\theta}|^2 + |E_{s,\phi}|^2)}{4\pi C_{\text{sca}}} \tag{27}$$

It is important to recognize that the angles θ and ϕ are not defined in the traditional sense—in that $\theta = 0$ does not correspond to the propagation direction of the incident radiation. By performing a suitable rotation of coordinate axes,[9] scattering angles θ', ϕ' can be defined so that $\theta' = 0$ denotes the incident propagation direction and $\phi' = 0$ corresponds to the

polarization state of the incident electric vector. The appropriate transformation is

$$\begin{aligned} \cos\theta &= \cos\beta\cos\theta' - \sin\beta\sin\theta'\cos(\phi' + \gamma) \\ \sin\theta\cos\phi &= \sin\theta'\cos(\phi' + \gamma) + \sin\beta\cos\theta' \end{aligned} \tag{28}$$

Note that, in terms of θ and ϕ, the forward direction is given by $\theta = \beta$ and $\phi = 0$.

The absorption efficiency of the particle is given by the difference of extinction and scattering

$$Q_{abs} = Q_{ext} - Q_{sca} \tag{29}$$

Alternatively, the absorption efficiency can be obtained directly from the field coefficients pertaining to sphere 2—since sphere 2 will be (for the system considered here) the sole absorber of the system. From a direct integration of the internal radiative intensity over the surface of sphere 2, the following equation can be obtained[9]:

$$Q_{abs} = \frac{4}{|m_2|^2 x_1^2} Re \sum_{m,n} E_{mn}\psi_n'(m_2x_2)\psi_n^*(m_2x_2) \times (m_2^*|d_{mn,2}|^2 + m_2|c_{mn,2}|^2) \tag{30}$$

in which the internal field coefficients for sphere 2 are related to the scattering coefficients by

$$d_{mn,2} = a_{mn,2}\frac{\bar{d}_{n,2}}{\bar{a}_{n,2}}, \qquad c_{mn,2} = b_{mn,2}\frac{\bar{c}_{n,2}}{\bar{b}_{n,2}} \tag{31}$$

Numerical Issues

The number of orders N_i that must be included in the field expansions for each of the two spheres is determined simply by examining the convergence of the computed efficiencies. It was found that the criterion specified by Bohren and Huffman for isolated spheres,[4] i.e.,

$$N_i = x_i + 4x_i^{1/3} + 2 \tag{32}$$

provided scattering and absorption efficiencies that were within 0.5% on a relative basis of the converged ($N_i \to \infty$) values.

Since we are interested in the absorption properties of the system for a number of different incident directions, we chose matrix inversion as the solution method for the scattering coefficients. In a condensed form, the system of equations given by Eqs. (9–12) can be expressed for each degree m as

$$\begin{bmatrix} I & \bar{F}^1 J^{1-2} \\ \bar{A}^2 J^{2-1} & I \end{bmatrix}_m \begin{bmatrix} d^1 \\ a^2 \end{bmatrix}_m = \begin{bmatrix} \bar{D}^1 p \\ 0 \end{bmatrix}_m \tag{33}$$

In Eq. (33), I is the identity matrix, $\bar{F}^1$ is a diagonal matrix having sequential elements of $\bar{f}_{n,1}$, $\bar{g}_{n,1}$, with n running from $|m|$ to N_1, and $\bar{D}^1$ and $\bar{A}^2$ are similar diagonal matrices constructed from the quantities $\bar{d}_{n,1}$, $\bar{c}_{n,1}$ and $\bar{a}_{n,2}$, $\bar{b}_{n,2}$, respectively. The matrices J consist of 2 × 2 blocks for each order n, the elements of which are given by

$$J_{nl}^{1-2} = (-1)^{n+l}\begin{bmatrix} A_{mlnn} & -B_{mlnn} \\ -B_{mlnn} & A_{mlnn} \end{bmatrix} \tag{34}$$

$$J_{nl}^{2-1} = \begin{bmatrix} A_{mlnn} & B_{mlnn} \\ B_{mlnn} & A_{mlnn} \end{bmatrix} \tag{35}$$

The vectors a^2, d^1 and p represent the scattering, internal, and incident field coefficients ($a_{mn,2}$, $b_{mn,2}$), ($d_{mn,1}$, $c_{mn,1}$), and (p_{mn}, q_{mn}), respectively. For each degree m, the number of coefficients for each of the spheres will be given by $M_i = 2[N_i + 1 - \max(1, |m|)]$. Note that this implies that the J matrices are not square; J^{1-2} will have M_1 rows and M_2 columns, and J^{2-1} will have the opposite. For our calculations, the size parameter of sphere 1 will typically be several times greater than that of sphere 2. Consequently, M_1 can be significantly greater than M_2. Because of this, the matrix inversion process can be speeded up by first formally factoring out d^1 in Eq. (33), resulting in the $M_2 \times M_2$ system of equations:

$$[I - \bar{A}^2 J^{2-1}\bar{F}^1 J^{1-2}]a^2 = -\bar{A}^2 J^{2-1}\bar{D}^1 p \tag{36}$$

Gaussian elimination[13] is then used to obtain the inverse matrix of the above system (again, for each degree m). For a given incident direction, the vector p is determined from Eq. (6), and the scattering coefficients making up a^2 are calculated. The internal field coefficients in d^1 are then obtained from

$$d^1 = \bar{D}^1 p - \bar{F}^1 J^{1-2} a^2 \tag{37}$$

Finally, the scattering coefficients $a_{mn,1}$, $b_{mn,1}$ are calculated using Eqs. (13) and (14). If only the absorption properties of the particle are desired, it is not necessary to compute the coefficients for sphere 1, as Eq. (30) can be used directly once a^2 is calculated.

Calculations were performed on a 486-based PC using a double precision Fortran 77 code. To give an indication of the time required for computation, calculation of the efficiencies for unpolarized radiation (obtained from the average of γ = 0- and 90-deg results) at 181 scattering angles for $x_1 = 35$, $x_2 = 3.5$ ($N_1 = 50$ and $N_2 = 11$) required approximately 8 min.

Results

In keeping with the heat transfer application of this study, the material comprising sphere 1 should be transparent in the visible and near to mid-ir wavelengths. We accordingly chose the refractive index for sphere 1 m_1 to be real (i.e., $m_1 = n_1$) and equal to 1.45 or 1.7, which correspond to visible values for crystalline quartz and sapphire, respectively. The refractive index of sphere 2 was taken to be $m_2 = 2 + 1i$, which corresponds to graphite. Again, we remain oblivious to the feasibility of producing eccentric, overlapping spheres of these materials; in this article we intend only to examine the radiative behavior of the hypothetical particles. In addition, if the particles were bound in a matrix of refractive index m_0, the values of m_1 and m_2 used in the calculations would be the material refractive index divided by m_0. In the following we also take the incident radiation to be unpolarized, and the corresponding properties were obtained from the average of results calculated for γ = 0 and 90 deg.

We begin with a qualitative presentation of the effects of the absorbing inclusion on the field inside the particle. To do this, it is useful to examine the internal electric field intensity $|E_i|^2$, which can be used to infer the distribution and strength of radiant intensity within the system. The intensity distributions for isolated (i.e., noninteracting) absorber and focuser particles are given in Fig. 2, in which the focuser (Fig. 2a) has $x = 20$, $m = 1.7$, and the absorber (Fig. 2b) has $x = 5$, $m = 2 + 1i$. The vertical scale represents $|E_i|^2$ in arbitrary units, and the horizontal axis denotes the z axis of the sphere in units of kz. Incident radiation is propagating in the positive z direction. As has been seen in several previous works,[5] the nonabsorbing sphere acts to concentrate the radiation about the surface immediately opposite the point of incidence. By placing an absorbing sphere within this focal region, the net intensity upon the absorber is significantly increased. This is seen in Figs. 3a and 3b, which presents $|E_i|^2$ for the two-sphere system comprised of the same spheres as in Fig. 2. The absorber is located against the inside surface opposite the point of incidence (i.e., $X_{1-2} = 15$ and $\beta = 0$ deg). Figure 3a shows the intensity distribution for the entire

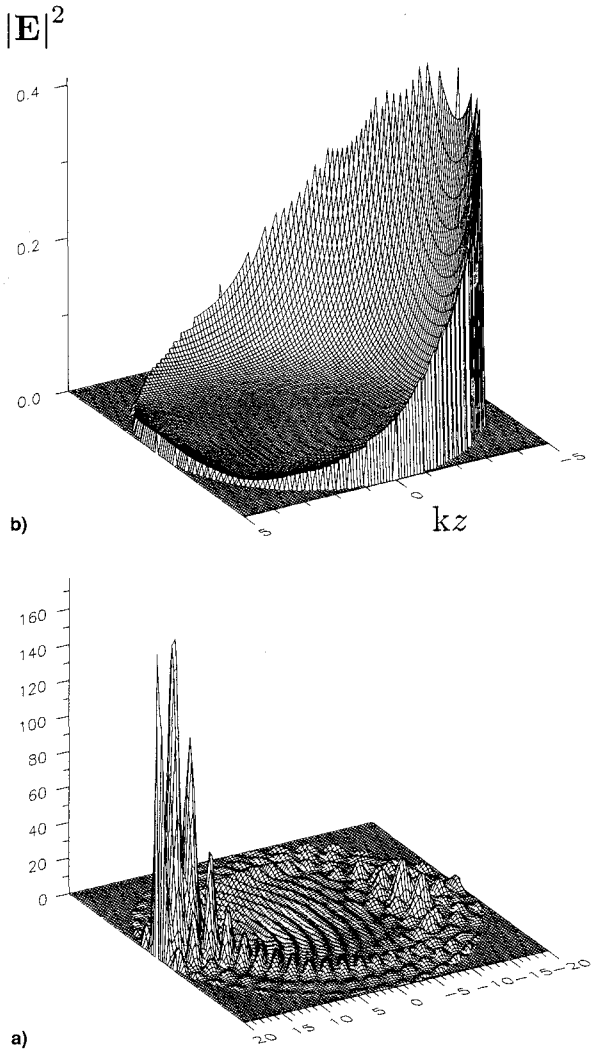

Fig. 2 Electric field intensity for isolated spheres of a) $x = 20$, $m = 1.7$ and b) $x = 5$, $m = 2 + 1i$.

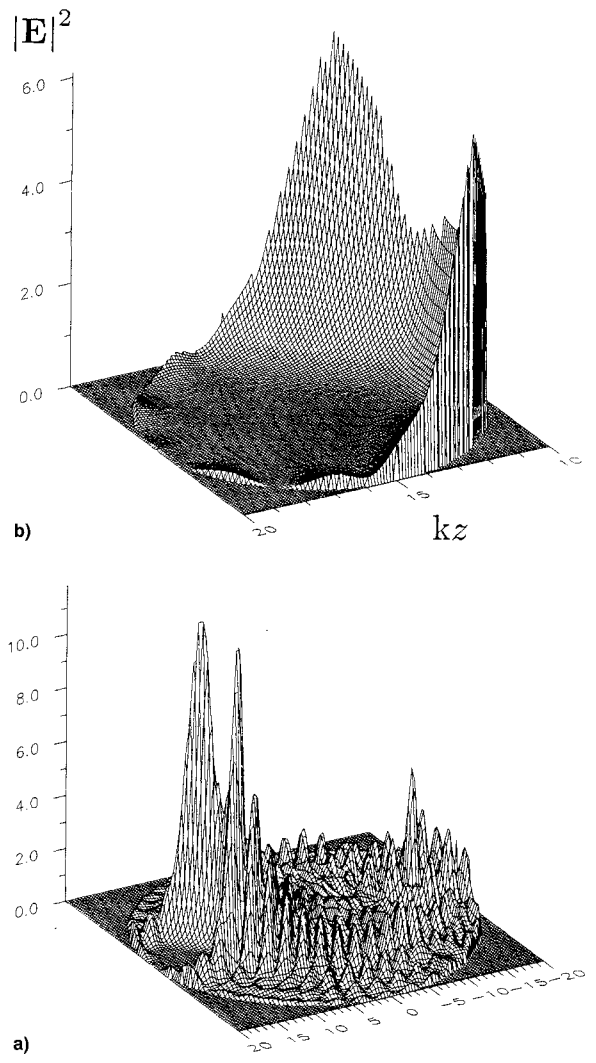

Fig. 3 a) Electric field intensity for a two-sphere system of the spheres in Fig. 2 and $X_{1-2} = 15$, $\beta = 0$ deg and b) detail of the field within sphere 2.

system, whereas Fig. 3b presents a detail of the intensity solely within the absorber. Comparison of Figs. 2b and 3b (note the scale change) indicates that the focused configuration results in peak intensities in the absorber that are around 10 times greater than that for the isolated absorber. By rotating the angle of incidence the absorber is removed from the focal spot of the nonabsorber, and the intensity within the absorber decreases. This is seen in Figs. 4a and 4b, which present the same configuration as in Fig. 3, except with $\beta = 30$ deg.

To quantify the effect of focusing on the particle absorption, we first examine the dependence of efficiency on β for a fixed ratio of x_2 to x_1. Results of the calculations appear in Fig. 5, in which Q_{abs} and Q_{sca} are plotted vs β for several values of x_1, and with $x_2/x_1 = 0.1$, $m_1 = 1.7$ and $X_{1-2} = x_1 - x_2$ (sphere 2 touching the boundary of 1). As expected, the absorption efficiency is highest for $\beta = 0$, which results in the focusing of radiation onto sphere 2. Values for Q_{abs} at $\beta = 0$ peak at around 0.83 for $x_1 = 15$ and 30, and drop to 0.77 for $x_1 = 50$. The peak values of Q_{abs} coincide with $x_2 = 1.5$ and 3.5—for which strongly absorbing spheres attain a maximum in Q_{abs}.[4] As x_1 increases, the distribution of Q_{abs} becomes more anisotropic, and oscillations in Q_{abs} with β are also damped out. The increasing anisotropy of Q_{abs} with x_1 is to be expected, for as sphere 1 becomes large with respect to λ, the field intensity within the sphere becomes more concentrated towards the forward regions of the sphere.

Figure 5 dramatically illustrates the degree to which the eccentric sphere system can produce a nonuniform absorption efficiency. For the larger spheres ($x_1 = 35, 50$), the absorption efficiency falls off by nearly 2 decades within 20 deg of the $\beta = 0$ direction. For larger incident angles, Q_{abs} never exceeds around 1% of the $\beta = 0$ value. These results are entirely consistent with previous finding by Fuller for carbon particles aggregated to sulfate or water droplets.[1,2] The extent to which the focusing of sphere 1 increases the absorption of sphere 2 can be seen by redefining the efficiency with respect to sphere 2. For the $x_1 = 50$ case, the absorption efficiency of 2 under the focused condition would be approximately $0.8 \times x_1^2/x_2^2 = 80$, which is roughly 80 times greater than the value for sphere 2 had it been isolated. Indeed, had sphere 1 been as strongly absorbing as sphere 2, its absorption efficiency would be only around 20% greater than that attained through focusing onto 2, yet sphere 2 occupies only 0.1% of the volume of 1.

Calculations for larger values of x_1 resulted in distributions of Q_{abs}, with β that were not appreciably different from that given for $x_1 = 50$. In addition, placing sphere 2 at positions closer to the origin of 1 produced, for the specific case of $m_1 = 1.7$, both a decrease in peak Q_{abs} and a less anisotropic distribution in Q_{abs} with β.

The computed extinction efficiencies were, for the choice of parameters in Fig. 5, found to be largely uneffected by β and equal to within 5% of the isolated value for sphere 1. Since $Q_{sca} = Q_{ext} - Q_{abs}$, the dip in scattering efficiency Q_{sca}

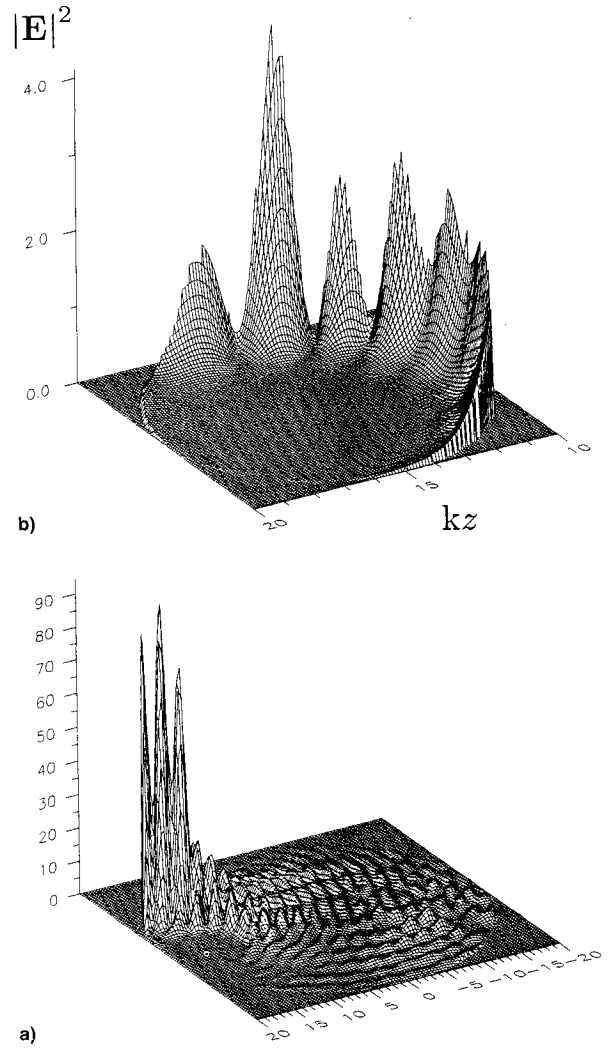

Fig. 4 a) Electric field intensity for a two-sphere system of the spheres in Fig. 2 and $X_{1-2} = 15$, $\beta = 30$ deg and b) detail of the field within sphere 2.

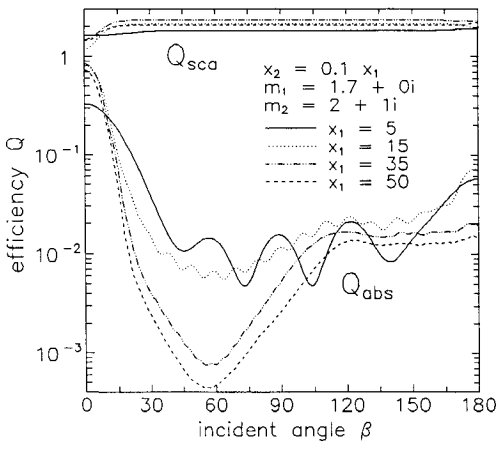

Fig. 5 Absorption and scattering efficiency vs β, with x_1 as a parameter, for fixed x_2/x_1.

at the forward direction is due entirely to the effect of increased absorption.

In the design of an "ideal" anisotropic absorbing sphere, one would want the absorption in the forward direction to be high, and the absorption "band" about the forward direction to be narrow. The results in Fig. 5 suggest that these criteria are better satisfied for relatively large-size parameters of the focusing sphere. To investigate the role of size parameter x_2

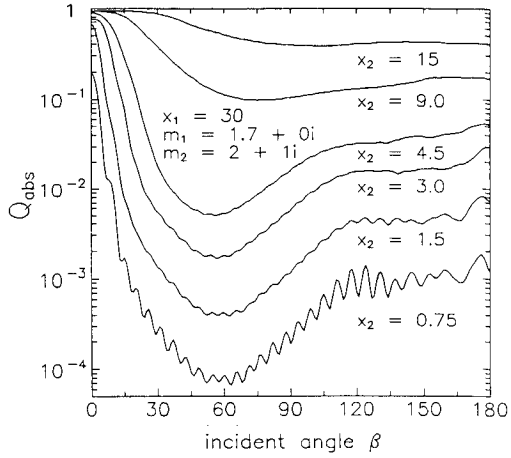

Fig. 6 Absorption efficiency vs β, with x_2 as a parameter, for fixed x_1.

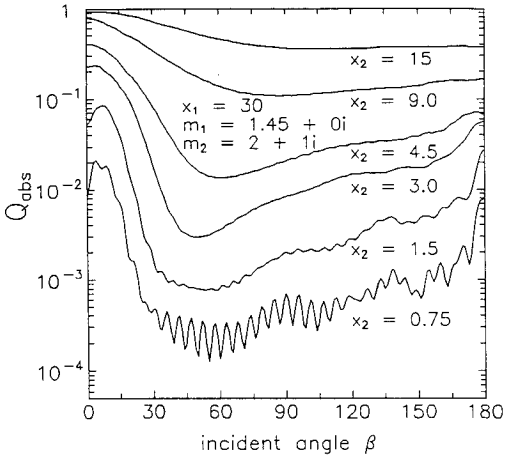

Fig. 7 Absorption efficiency vs incident angle, for same parameters as Fig. 3 except $m_1 = 1.45$.

on the absorption distribution, we performed similar calculations, yet held x_1 fixed at 30 and varied x_2. Results for these calculations appear in Fig. 6. These results indicate that as x_2 decreases for fixed x_1, the absorption bandwidth about $\beta = 0$ decreases, yet the peak absorption decreases as well. In addition, for x_2 greater than a certain fraction of x_1 (0.15 in the case of Fig. 6), the peak absorption efficiency attains a limiting value of around 0.9—which corresponds, again, to what one would expect for large absorbing spheres. However, the degree of anisotropy in Q_{abs} diminishes as x_2 increases. For $x_2 = 4.5$, the backward ($\beta = 180$ deg) absorption is around 5% of the forward absorption, whereas for $x_2 = 15$, the ratio is approximately 50%. Consequently, the results suggest that an "optimum" value of x_2/x_1 exists, which would be the smallest ratio that gives a forward absorption efficiency near the limiting value of unity. From inspection of Fig. 6, we would gather that the optimum x_2/x_1 ratio, for the particular values of refractive index, is on the order of 0.05–0.15.

Further calculations indicate that the refractive index of sphere 2 does not appreciably affect the results as long as the imaginary part is relatively large (i.e., the material is strongly absorbing). Results obtained for the same parameters of Fig. 5 for $x_1 = 30$, except with $m_2 = 1.5 + 0.2i$ were within 5% of those shown. However, the refractive index of sphere 1 does have an appreciable effect on the strength and anisotropy of absorption. Presented in Fig. 7 are results calculated using the parameters of Fig. 5, except with $m_1 = n_1 = 1.45$, which corresponds again to the value for crystalline quartz in the visible. For this refractive index the peak value of Q_{abs} is

considerably less than that attained for $n_1 = 1.7$. For example, the $\beta = 0$ absorption efficiency for $x_2 = 3$ is, at around 0.25, approximately one-third that for the $n_1 = 1.7$ case. Furthermore, the absorption band about $\beta = 0$ is not nearly as narrow as it is for the larger n_1.

The results would seem to imply that the focusing ability of the sphere would increase with n_1, but additional calculations reveal that, for the configurations in the previous figures, the maximum Q_{abs} actually occurs for n_1 in the vicinity of 2.0, and for larger n_1 the absorption drops. An explanation for this behavior, which is drawn from geometrical optics,[5] considers the refraction of rays incident at the sphere boundary. As n_1 increases, the rays entering the sphere surface are increasingly bent towards the center of the sphere. This behavior is graphically shown in Figs. 8a and 8b, in which the electric field intensity $|E_i|^2$ is presented for the same particle configuration as in Fig. 3, except for $m_1 = n_1 = 2$ (Fig. 2a) and 2.2 (Fig. 2b). As can be seen by comparison of Figs. 3a, 8a, and 8b, the point of peak intensity moves inwards (and away from the absorber) as n_1 increases. Indeed, calculations indicate that for n_1 greater than 2 and relatively large x_1, the maximum Q_{abs} occurs when the absorbing sphere is somewhat removed from the interior surface of sphere 1. For such situations, however, the distribution of Q_{abs} with β is considerably more uniform than is the case when the absorbing sphere is located at the surface. The same argument can be extended to the configuration where sphere 2 is located external to 1.[1] For this case, decreasing n_1 will move the focal spot away from the sphere.

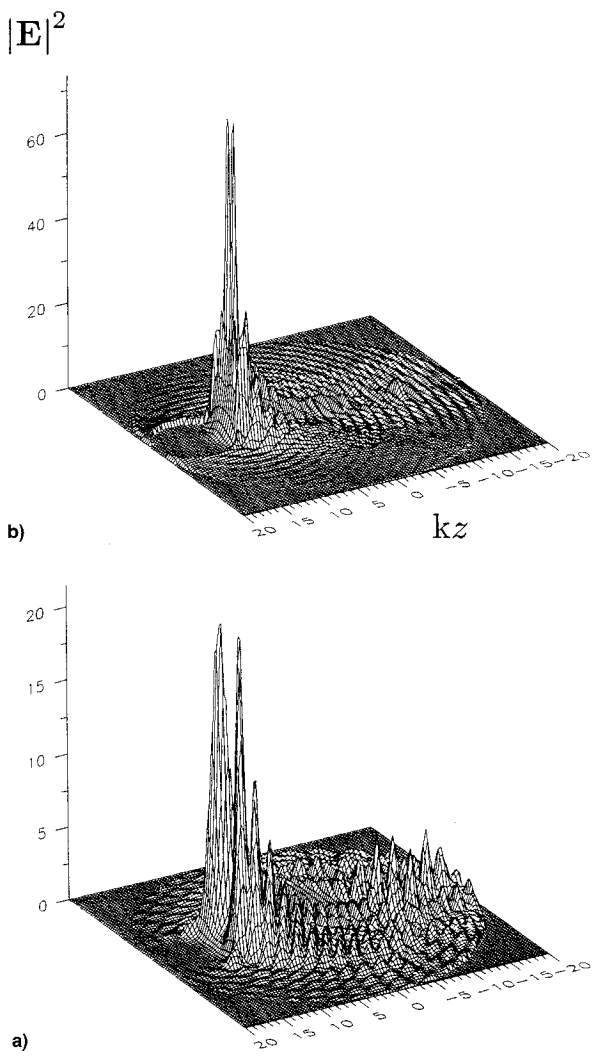

Fig. 8 Field intensities within the two sphere system of Fig. 2, except with m_1 = a) 2 and b) 2.2.

An additional factor to consider is a small, but finite, imaginary part of the refractive index of sphere 1. Either through inherent impurities in the focusing material or leaching of the absorber into the focuser, the material making up the focuser could possess nonzero absorption. To investigate this effect, we calculated distributions of Q_{abs} with β for $x_1 = 35$, $x_2 = 3.5$, $X_{1-2} = x_1 - x_2$, $m_1 = 2 + 1i$, and $m_1 = 1.7 + ik_1$ with $k_1 = 0$, 10^{-5}, 10^{-4}, and 10^{-3}. Results of these calculations are given in Fig. 9. As expected, a nonzero k_1 has the most immediate effect on the minimum Q_{abs}—which occurs for β between 30–90 deg. For $k_1 = 10^{-4}$ and greater, the absorption of the focuser has a significant effect on the absorption in the backwards (i.e., $\beta > 90$ deg) directions. The effect of a nonzero k_1 on Q_{abs} would be proportionally greater for focusers having larger values of x_1, because the radiation propagating though the focuser would travel across a larger path length and, thus, be subject to increased attenuation through absorption. It is interesting to note that the absorption of the focuser has a relatively smaller effect on absorption in the focused configurations ($\beta < 20$ deg) than it does on the backwards directions. This behavior likely arises from the effect of the absorber on multiple reflections of radiation within the focuser. When the absorber is in the focal spot, a relatively large fraction of the radiation entering into the focuser is absorbed by the inclusion during the first "pass" of the radiation through the focuser. Consequently, less radiation is available to undergo multiple reflections and subsequent absorption within the focuser itself.

As mentioned above, the presence of the small, absorbing particle has a significant effect on the scattering efficiency only when β is near zero. As expected, the effect on the phase function and backscattering efficiency is also greatest for this condition. Given in Fig. 10 are results for the backscattering efficiency of a particle having $x_1 = 35$, $x_2 = x_1/10$, and $m_1 = 1.7$ and 1.45. The other parameters are the same as in previous plots. Presented also are Q_{back} values for a homogeneous sphere having the same m and x as sphere 1. Note that, for β greater than around 20 deg, the backscattering efficiency for $m_1 = 1.7$ is essentially equivalent to that for the homogeneous sphere, yet for smaller β, Q_{back} drops to one-tenth of the homogeneous sphere value. The absorbing particle has a more significant effect on the backscattering efficiency when $m_1 = 1.45$, yet again, Q_{back} for $\beta > 20$ deg is roughly equivalent to that for the homogeneous sphere. However, Q_{back} is now greatest for $\beta = 0$. Similar results were found for the scattering phase function—in that Φ for $\beta > 20$ deg is very similar to that predicted for a homogeneous sphere with refractive index m_1, providing that x_2 is small relative to x_1 (i.e., $x_2 \leq x_1/10$). For smaller incident angles, the distribution of scattering becomes weighted slightly more towards the forward direction—yet the deviation from the homogeneous sphere case is not ap-

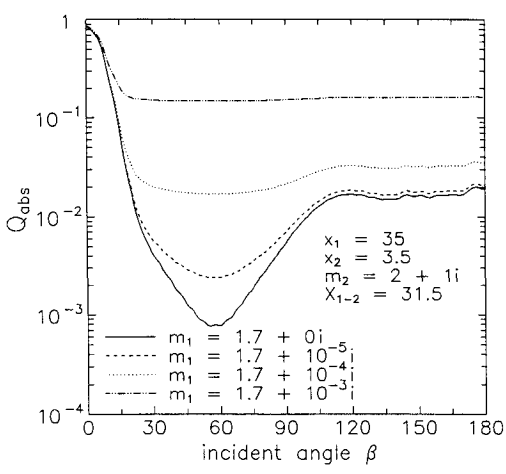

Fig. 9 Effect of nonzero imaginary part of m_1 on absorption distribution.

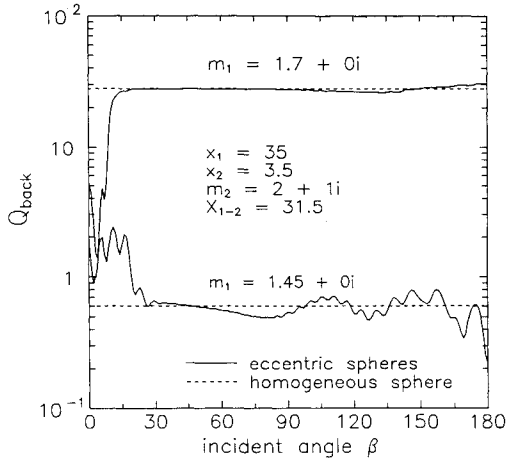

Fig. 10 Backscattering efficiency vs incident angle, for eccentric spheres and homogeneous spheres having refractive index m_1.

preciably significant. Because of this, it appears reasonable to approximate the scattering phase function from the particle as being independent of β and equal to that of the homogeneous sphere.

Conclusions

The results presented here demonstrate that, by imbedding a small absorbing sphere within a larger, nonabsorbing sphere, the absorption efficiency of the particle as a whole can be extremely sensitive to the direction of incident radiation. It should be emphasized that the analysis was exact, and we are fully confident that real particles of the same form investigated here would display the same absorption characteristics. By Kirchoff's law,[4] we would also expect the spectral thermal emission from an isothermal particle to follow the same directional distribution as the absorption cross section.

The radiative properties of a hypothetical medium comprised of such particles, all equally sized and oriented in the same direction, are intriguing to consider. The absorption coefficient of the medium, which is given by $\kappa_\lambda = \pi a_1^2 N_p Q_{abs}$, where N_p is the particle number density, would be equally as anisotropic as the absorption cross section. It would thus be expected that the transfer of radiation through the medium would be strongly dependent on direction. A slab of the medium, e.g., would have different radiative transmittance properties depending upon whether the incident radiation originated from the high or the low absorbing side. The same would be true for the thermal emission from the slab. Since, however, the particles appreciably scatter radiation, it is necessary to perform a detailed analysis of radiative transfer within the medium to elucidate its potential properties. We have undertaken such an analysis in a companion article.[3]

Appendix: Addition Coefficients

Although explicit relations exist for the addition coefficients A and B,[14] they are most efficiently calculated via recurrence relations. Details of the derivation of the recurrence relations can be found in Mackowski,[9] only the working relations for axial translation are given here. The vector harmonic addition coefficients can be calculated from the scalar harmonic addition coefficients C_{mlmn} via

$$A_{mlmn} = X_{1-2}\left[\frac{n+m+1}{(n+1)(2n+3)} C_{mlmn+1} + \frac{n-m}{n(2n-1)} C_{mlmn-1}\right] + C_{mlmn} \tag{A1}$$

$$B_{mlmn} = \frac{imX_{1-2}}{n(n+1)} C_{mlmn} \tag{A2}$$

The scalar addition coefficients, in turn, can be obtained from the following recurrence relations:

$$\frac{1}{2l+1}[C_{ml-1mn} + C_{ml+1mn}] = \frac{1}{2n-1} C_{m-1lm-1n-1} + \frac{1}{2n+3} C_{m-1lm-1n+1} \tag{A3}$$

$$\frac{1}{2l+1}[(l+m)(l+m+1)C_{ml-1mn} + (l-m)(l-m+1)C_{ml+1mn}] = \frac{(n-m)(n-m-1)}{2n-1} C_{m+1lm+1n-1} + \frac{(n+m+1)(n+m+2)}{2n+3} C_{m+1lm+1n+1} \tag{A4}$$

$$\frac{1}{2l+1}[(l+m)C_{ml-1mn} - (l-m+1)C_{ml+1mn}] = -\frac{n-m}{2n-1} C_{mlmn-1} + \frac{n+m+1}{2n+3} C_{mlmn+1} \tag{A5}$$

In the above equations, it is understood that the addition coefficients A_{mnml}, B_{mlmn}, and C_{mlmn} are zero if $|m| > l$ or $|m| > n$.

Starting values for the above recurrence relations are obtained explicitly from the formula

$$C_{00mn} = (-1)^{n+m}(2n+1) j_n(X_{1-2}) \tag{A6}$$

It should be noted that the recurrence relations are unconditionally stable. However, to calculate C_{mlmn} up to $l = n = N$ orders, it is necessary to begin with C_{00mn} calculated to $l = 2N$ orders.

Useful symmetry relations for the addition coefficients are

$$A_{-ml-mn} = (-1)^{n+l}\frac{(2n+1)l(l+1)}{(2l+1)n(n+1)} A_{mnml} = \frac{(n+m)!(l-m)!}{(n-m)!(l+m)!} A_{mlmn}$$

$$B_{-ml-mn} = -(-1)^{n+l}\frac{(2n+1)l(l+1)}{(2l+1)n(n+1)} B_{mnml} = -\frac{(n+m)!(l-m)!}{(n-m)!(l+m)!} B_{mlmn} \tag{A7}$$

References

[1]Fuller, K. A., "Scattering and Absorption Cross Sections of Compounded Spheres. II. Calculations for External Aggregation," *Journal of Atmospheric Science* (submitted for publication).

[2]Fuller, K. A., "Scattering and Absorption by Inhomogeneous Spheres and Sphere Aggregates," *Proceedings of SPIE Conference 1862, Laser Applications in Combustion and Combustion Diagnostics*, edited by L. C. Liou, 1993, pp. 249–257.

[3]Jones, P. D., and Mackowski, D. W., "Non-Kirchhoff Surface Using Media with Directionally Varying Absorption Efficiency," *Journal of Thermophysics and Heat Transfer*, Vol. 9, No. 2, 1995, pp. 202–209.

[4]Bohren, C. F., and Huffman, D. R., *Absorption and Scattering of Light by Small Particles*, Wiley, New York, 1983.

[5]Chowdury, D. Q., Barber, P. W., and Hill, S. C., "Energy-Density Distribution Inside Large Nonabsorbing Spheres by Using Mie Theory and Geometrical Optics," *Applied Optics*, Vol. 31, No. 18, 1992, pp. 3518–3523.

[6]Brunning, J. H., and Lo, Y. T., "Multiple Scattering of EM Waves by Spheres. Part I. Multipole Expansion and Ray-Optical Solutions," *IEEE Transactions on Antennas and Propagation*, Vol. AP-19, No. 3, 1971, pp. 378–390.

[7]Borghese, F., Denti, P., Saija, R., and Toscano, G., "Multiple Electromagnetic Scattering from a Cluster of Spheres. I. Theory," *Aerosol Science and Technology*, Vol. 3, No. 2, 1984, pp. 227–235.

[8]Fuller, K. A., "Optical Resonances and Two-Sphere Systems," *Applied Optics*, Vol. 30, No. 33, 1991, pp. 4716–4731.

[9]Mackowski, D. W., "Analysis of Radiative Scattering for Multiple Sphere Configurations," *Proceedings of the Royal Society of London*, Vol. A433, 1991, pp. 599–614.

[10]Fikioris, J. G., and Uzunoglu, N. K., "Scattering from an Eccentrically Stratified Dielectric Sphere," *Journal of the Optical Society of America*, Vol. 69, No. 10, 1979, pp. 1359–1366.

[11]Borghese, F., Denti, P., Saija, R., and Sindoni, G., "Optical Properties of Spheres Containing a Spherical Eccentric Inclusion," *Journal of the Optical Society of America A*, Vol. 9, No. 8, 1992, pp. 1327–1335.

[12]Mackowski, D. W., Altenkirch, R. A., and Menguc, M. P., "Internal Absorption Cross Sections in a Stratified Sphere," *Applied Optics*, Vol. 29, No. 10, 1990, pp. 1551–1559.

[13]Press, W. H., Flannery, B. P., Teukolsky, S. A., and Vetterling, W. T., *Numerical Recipes*, Cambridge Univ. Press, Cambridge, England, UK, 1986.

[14]Cruzan, O. R., "Translational Addition Theorems for Spherical Vector Wave Functions," *Quarterly Applied Mathematics*, Vol. 20, No. 1, 1962, pp. 33–39.